A PARAMETRIC MODEL OF VERTICAL EDDY FLUXES IN THE ATMOSPHERE

JEAN-FRANÇOIS LOUIS

European Centre for Medium Range Weather Forecasts, Shinfield Park, Reading, Berks, U.K.

(Received 27 March, 1979)

Abstract. A scheme for the representation of the vertical eddy fluxes of heat, momentum and water vapour in a forecast model is presented. An important feature of the scheme is the dependence of the diffusion coefficients on the static stability of the atmosphere. Two tests are presented, using the scheme in a one-dimensional model: the simulation of the diurnal cycle, and the transformation of a polar air mass moving over the warm sea.

1. Introduction

This paper describes a method for the simulation of the vertical eddy fluxes of heat, momentum and moisture in a 10-day forecast model. For a short-range forecast (1 or 2 days), it is generally assumed that a very simple representation of the drag at the surface is sufficient to account for the effect of the boundary layer fluxes. When the forecast is extended to a week or 10 days, however, it is likely that a more detailed simulation of the vertical eddy fluxes of momentum, heat and water vapour is necessary.

Since there is very little experience in medium-range forecasting, we turned to the existing models of the general circulation of the atmosphere for guidance. A good review of the methods used in these models can be found in Bhumralkar (1975a). The eddy fluxes are most important in the turbulent boundary layer, where the profiles of wind and temperature vary rapidly with height, and the main choice to be made depends on the vertical resolution of the model in this region. One can either have a high resolution in the boundary layer – e.g., four or five model levels below 800 mb – and have a detailed representation of the vertical profile of the fluxes, making some closure assumption, or one can choose a low resolution – one or two levels – and make some assumption on the flux profiles themselves. In the latter case one usually assumes a linear profile for the fluxes between the ground and the top of the boundary layer, the height of the top being either constant or determined by the model (see, e.g., Deardorff (1972)). An example of the first choice, with a simple first-order closure (K theory), has been described by Smagorinsky *et al.* (1965).

In order to choose a parameterisation scheme it is necessary to consider the imperatives peculiar to a 10-day forecast, as well as the resources available. The first requirement is speed. Even with a very fast computer, to make a high-resolution (about 1.5 deg in the horizontal and 15 levels) 10-day integration in less than 10 hours, it is necessary to keep the parameterisation of all the physical processes at a simple level. On these grounds we decided to reject higher order closure methods.

Boundary Layer Meteorology **17** (1979) 187–202. 0006–8314/79/0172–0187$02.40.

The choice between a detailed representation of the boundary layer or a bulk method is more difficult. We felt, however, that the introduction of auxiliary prognostic variables (height of the boundary layer, temperature jump at the top) which cannot be easily initialized or verified, might produce some incorrect feed-back mechanisms in the model. Hence we preferred a detailed boundary layer where the magnitude of the eddy fluxes is related to the variables of the model, using the diffusion principle.

We feel that an accurate description of feed-back mechanisms is very important in a prediction model. If a 10-day forecast is to be successful, we must be able to simulate correctly those situations where physical processes interact with each other and with the atmospheric motions to alter these motions significantly, and create new developments in the synoptic fields. We do not want the physical parameterisation to force the model quickly towards its climatological mean state. Rather the model should be able to respond correctly to the physical forcing, especially in extreme situations. In other words, we must emphasize changes in the weather rather than the mean state.

Following these ideas, it is clear that it is not sufficient to have a boundary-layer scheme where the diffusion coefficients depend only on the wind shear as in the Prandtl formulation; they must also depend on the static stability of the atmosphere, so that thermally as well as mechanically forced turbulence can be simulated. Furthermore, the vertical extent of the turbulent region must be allowed to vary, and the possibility of turbulence in regions of high shear in the free atmosphere must be considered. Finally, these requirements must be fulfilled with a scheme containing as few adjustable parameters as possible.

In the next section we describe the scheme proposed for the parameterisation of the vertical eddy fluxes in a medium-range forecast model. We will then show the results of some one-dimensional experiments designed to test the ability of the scheme to simulate the diurnal cycle and to respond to intense forcing. The performance of this scheme in a global forecast model is being investigated at the present time and results of these tests will be presented elsewhere.

2. The Parameterisation Scheme

A. The surface fluxes

The chosen parameterisation scheme for the surface fluxes is based on Monin–Obukhov (1954) similarity theory. This theory has been widely discussed in the meteorological literature (see, e.g., Dyer (1974) or Arya and Sundararajan (1976)) and it is well supported by experimental evidence (Businger *et al.*, 1971; Phelps and Pond, 1971; Högström and Smedman-Högström, 1974, among others) at least for neutral and unstable conditions.

Following Paulson (1970) and Barker and Baxter (1975), we integrate the flux-profile relationships between the roughness length z_0 and the height z of the

lowest model level. We obtain the relations:

$$u(z) = \frac{u_*}{k}[\ln(z/z_0) - \psi_m(z/L) + \psi_m(z_0/L)] \tag{1}$$

$$\Delta\theta = \theta(z) - \theta_0 = R\frac{\theta_*}{k}[\ln(z/z_0) - \psi_h(z/L) + \psi_h(z_0/L)] \tag{2}$$

where k is the Von Karman constant, u and θ are the wind and potential temperature at height z, θ_0 the potential temperature at z_0 (taken at the same as the ground temperature) and R is a constant. The scaling velocity and temperature are defined from the vertical eddy fluxes of momentum $\overline{w'u'}$ and sensible heat $\overline{w'\theta'}$:

$$u_* = \sqrt{|\overline{w'u'}|} \tag{3}$$

$$\theta_* = -\overline{w'\theta'}/u_*\,, \tag{4}$$

and L is the Monin–Obukhov scale height:

$$L = \frac{\bar{\theta}u_*^2}{kg\theta_*} \tag{5}$$

where g is the gravity. A relation similar to (2) is assumed to hold for water vapour as well.

If we use Businger's functions for the flux-profile relationships, the functions ψ have the following form:

$$\psi_m(\zeta) = \ln\left[\left(\frac{1+x}{2}\right)^2\left(\frac{1+x^2}{2}\right)\right] - 2\arctan x + \frac{\pi}{2} \tag{2}$$

with

$$\begin{aligned} x &= (1-\gamma_m\zeta)^{1/4} \quad \text{for unstable conditions and} \\ \psi_m(\zeta) &= -\beta\zeta \qquad\qquad \text{for stable conditions}\,, \end{aligned} \tag{7}$$

$$\psi_h(\zeta) = \ln\left[\left(\frac{1+y}{2}\right)^2\right] \tag{8}$$

with

$$\begin{aligned} y &= (1-\gamma_h\zeta)^{1/2} \quad \text{for unstable conditions and} \\ \psi_h(\zeta) &= -\beta\zeta/R \qquad\quad \text{in stable conditions}\,. \end{aligned} \tag{9}$$

In order to get the eddy fluxes u_*^2 and $u_*\theta_*$ from the model variables u and $\Delta\theta$, one must eliminate L from (1) and (2), using (5). This is not possible analytically in unstable conditions, but it can be done numerically, by iterations. Such a method has been used in some boundary-layer models (e.g., Delsol *et al.* (1971); Busch *et al.* (1976)). However, for maximum speed of computation, we want to avoid iterative

methods. We then proceed as follows. Substituting (1) and (2) into (5), we obtain:

$$L = \frac{\bar{\theta}u^2}{g\Delta\theta} \frac{[\ln(z/z_0) - \psi_m(z/L) + \psi_h(z_0/L)]}{[\ln(z/z_0) - \psi_m(z/L) + \psi_m(z_0/L)]^2}. \tag{10}$$

This is an implicit relationship between the Monin–Obukhov scale height L and the bulk Richardson number for the layer

$$\mathrm{Ri}_B = \frac{gz\Delta\theta}{\bar{\theta}u^2}. \tag{11}$$

We can then write, formally:

$$u_*^2 = a^2 u^2 F_m\left(\frac{z}{z_0}, \mathrm{Ri}_B\right) \tag{12a}$$

$$u_*\theta_* = \frac{a^2}{R} u\Delta\theta F_h\left(\frac{z}{z_0}, \mathrm{Ri}_B\right) \tag{12b}$$

where

$$a^2 = k^2 \Big/ \left(\ln\frac{z}{z_0}\right)^2 \tag{13}$$

is the drag coefficient in neutral conditions. The constant R, ratio of the drag coefficients for momentum and heat in the neutral limit, was estimated by Businger *et al.* (1971) to be 0.74. The functions a^2F_m and a^2F_h have been computed numerically and are shown on Figure 1 (a) and (b) (solid lines) in terms of the Richardson number, for several values of z/z_0. If we can fit analytical formulae to these computed curves, we will then avoid the need to do the iterative computation at every time step of the integration. This is also more convenient than the use of nomograms or table look-up as proposed by Clarke (1970). Since the curves F_m and F_h are quite similar for momentum and heat, we will try to fit both with formulae of the same kind. In what follows, we will generally drop the indices m and h, keeping in mind that F may have different coefficients for momentum and heat.

Let us first consider the unstable case ($\mathrm{Ri}_B < 0$). In order to have a finite heat flux in the free convection limit (i.e., for $u = 0$), it can be seen from (11) and (12) that for u small, F must behave as $1/u$, i.e., as $|\mathrm{Ri}_B|^{1/2}$. On the other hand, the behaviour of F near neutral conditions ($\mathrm{Ri}_B = 0$) depends on the slope of the flux-profile relationship near neutrality. With these constraints, we found the following simplest analytical formula which fitted reasonably well the computed curves in the unstable case:

$$F = 1 - \frac{b\mathrm{Ri}_B}{1 + c|\mathrm{Ri}_B|^{1/2}}. \tag{14}$$

The numerical value of the coefficients b and c will be discussed later.

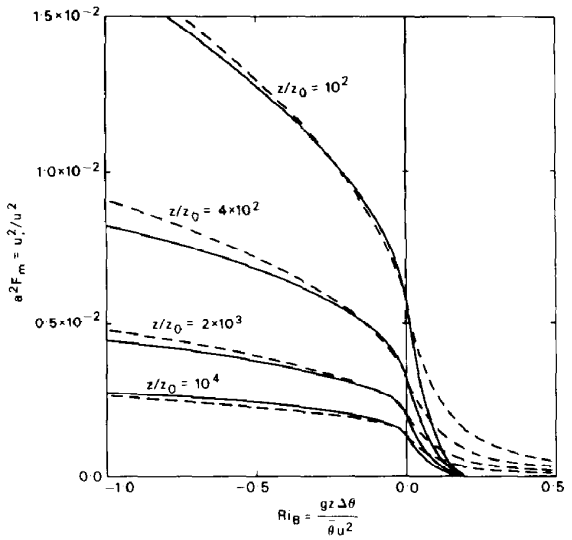

Fig. 1a. Drag coefficient for momentum, in terms of the bulk Richardson number and the roughness length. Computed by iterations: ———, using analytical formulae: – – – – –.

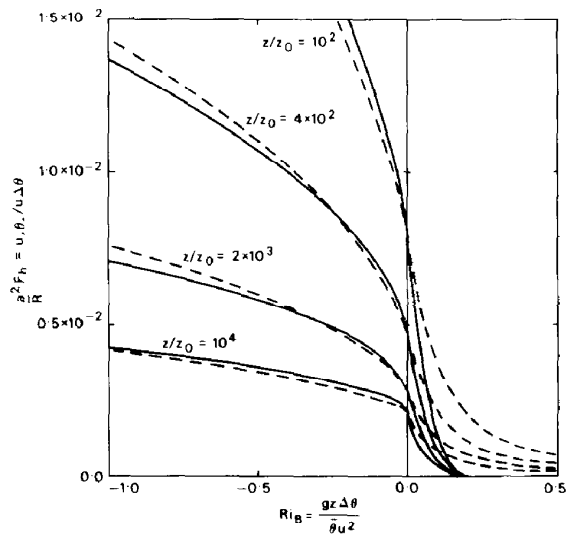

Fig. 1b. Same as Figure 1a, but for heat.

One might think that the treatment of the stable case should be simpler than the unstable one since, again using Businger's functions, (10) can be solved analytically for L. The solution is slightly complicated, but can be approximated very closely by a simple quadratic function up to the point where F vanishes, at a critical value of the bulk Richardson number of 0.21. Such a function was, in fact, used in our first experiments.

It turns out, however, that using a quadratic function for F in the stable case produces unrealistic results. We find that once the bulk Richardson number exceeds its critical value, the ground becomes energetically disconnected from the atmosphere and starts cooling by radiation at a faster rate than is actually observed. Unrealistically low night-time ground temperatures are produced. It can be argued that this difficulty comes from the finite vertical resolution of the model which cannot handle situations when the thickness of the turbulence layer becomes smaller than the lowest model level. In their review of the question, Carson and Richards (1978) suggest that a higher critical Richardson number (1.33) should be used. On the other hand, Merrill (1977) has observed intermittent turbulence even in situations where the Richardson number exceeded the critical value. Kondo *et al.* (1978) made the same observation and suggest that the linear flux-profile relationship in stable conditions should be modified to tend towards an asymptote at high Richardson numbers. Such a flux-profile would imply that the drag coefficient never vanishes.

In the light of our experiments, we adopted expressions of the following form for F in stable conditions:

$$F = 1/(1 + b' \mathrm{Ri}_B)^2 . \tag{15}$$

The values of the factors b, b' and c are rather uncertain because of the large scatter in the observations. We thought that for the sake of numerical stability, it might be better to make the first derivative of F continuous between the stable and unstable conditions. Hence we chose $b = 2b' = 9.4$.

In order to find the dependence of c with z, it is convenient to do a dimensional analysis in the free convection limit. If we assume that for free convection, the temperature gradient depends only on z, $g/\bar{\theta}$ and the heat flux $\overline{w'\theta'}$, then we can define a scaling temperature

$$\theta_* = \left(\frac{\overline{w'\theta'^2}\bar{\theta}}{zg} \right)^{1/3} \tag{16}$$

and write the flux-profile relationship:

$$\frac{z}{\theta_*} \frac{\partial \theta}{\partial z} = C \tag{17}$$

where C is a constant.

Integrating from z_0 to z and assuming that the heat flux is constant in this layer, we obtain:

$$\overline{w'\theta'} = C' \left(\frac{gz}{\theta} \right)^{1/2} \frac{\Delta\theta^{3/2}}{[(z/z_0)^{1/3} - 1]^{3/2}} . \tag{18}$$

Using (14) and taking the limit of (11) for $u \to 0$ we get

$$\overline{w'\theta'} = -u_*\theta_* = \frac{a^2 b}{Rc} \left(\frac{gz}{\bar{\theta}} \right)^{1/2} \Delta\theta^{3/2} \tag{19}$$

Comparing (18) and (19) yields, assuming $z \gg z_0$:

$$c = C^* a^2 b \left(\frac{z}{z_0}\right)^{1/2} . \tag{20}$$

For a best fit of the computed curves for F_m and F_h, we found $C^* = 7.4$ for momentum and 5.3 for the heat and moisture fluxes. The curves computed with formulae (14) and (15) are shown on Figure 1 (a) and (b), as dashed lines.

B. FLUXES ABOVE THE SURFACE LAYER

Above the surface layer, the eddy fluxes are computed as diffusive fluxes. The diffusion coefficient K depends on height, shear and stability. For the sake of continuity with the surface fluxes, the dependence of K with stability is assumed the same as that of the surface fluxes. We write then:

$$K_m = l^2 \left|\frac{\Delta v}{\Delta z}\right| F(\mathrm{Ri}) \tag{21}$$

and a similar formula for K_h.

We use the formula suggested by Blackadar (1962) for the mixing length l:

$$l = \frac{kz}{1 + \dfrac{kz}{\lambda}} \tag{22}$$

where the asymptotic mixing length λ is an adjustable parameter. In the experiments described below, it was taken as 100 m. The function F in (21) is the same as in (14) and (15) except that now the Richardson number is defined as

$$\mathrm{Ri} = \frac{g \Delta z \Delta \theta}{\bar{\theta} (\Delta v)^2} \tag{23}$$

where Δz is the thickness of the layer, and a similar dimensional argument as before shows that the coefficient c in (14) should now be:

$$c = C^* \frac{l^2 b [(z + \Delta z/z)^{1/3} - 1]^{3/2}}{z^{1/2} \Delta z^{3/2}} . \tag{24}$$

It should be noted that even though the mixing length l increases with height, the diffusion coefficient does not necessarily, since the normal stability of the atmosphere is such that the function F is very small above the boundary layer and keeps the diffusion coefficient to a very small value. Typically K is two or three orders of magnitude greater in the unstable boundary layer than in the free atmosphere. Only in case of very strong shear can K reach a significant value in the free atmosphere. In this model we use the same diffusion coefficient for water vapour mixing ratio as for heat.

3. Experiments

Some numerical experiments were undertaken to test this model's ability to simulate the diurnal cycle and to respond to unusually strong forcing. We will present here some results of two simulations: period 5 of the O'Neill experiment and a case of transformation of a polar air mass over the Norwegian Sea. These cases were chosen because, in both of them, the effect of large-scale advection was minimal and the evolution of the atmospheric structure could be simulated with a one-column model.

A. Diurnal cycle

Period 5 of the O'Neill experiment (Lettau and Davidson, 1957) was chosen because it is a well documented example of the diurnal variation of boundary-layer structure under clear sky. In this experiment we used the observed initial conditions, we assumed that the geostrophic wind is constant, and we forecast the ground temperature and moisture as well as the atmospheric structure. The radiative transfer model of Geleyn and Hollingsworth (1979) was used to compute the radiative forcing.

The ground temperature T_g and moisture W_g were predicted following Bhumralkar (1975b) and Deardorff (1978):

$$\frac{\partial T_g}{\partial t} = (F_R + F_H + LF_W)/C_T + (T_d - T_g)/\tau \tag{25}$$

$$\frac{\partial W_g}{\partial t} = (P + F_W)/C_W + (W_d - W_g)/\tau \tag{26}$$

with

$$W_g \leq W_{\max} \; ; \tag{27}$$

F_R, F_H and F_W are the fluxes of radiation, sensible heat and water vapour, respectively (positive downwards); P is precipitation, if any; T_d and W_d are given values of the temperature and moisture of the deep layer of the ground; C_T and C_W are the capacities for heat and moisture of the superficial layer which reacts to the diurnal cycle, whereas τ is the time scale for the restoring effect of the deep layer. If the soil moisture reaches $W_{\max}$, any excess water is eliminated by run-off. The mixing ratio at the ground surface q_0 is then related to the soil moisture and temperature:

$$q_0 = W_g q_{\text{sat}}(T_g)/W_{\max} \, . \tag{28}$$

Some of the constants in (25)–(28) can be deduced from measurements, but some are unknown and had to be adjusted. From the measured values of the thermal conductivity and heat capacity of the soil, we have $C_T = 5.5 \times 10^4$ kg s^{-2} K^{-1}; T_d and W_d were measured as 293.5 K and about 5% wet volume, respectively. We assumed that $C_W = 0.12$ m and $\tau = 1$ day. Several values of $W_{\max}$ were tried. Somewhat surprisingly the best simulation was obtained with $W_{\max} = W_d$. This would imply that at some depth below the surface, the soil would be saturated with only 5% water

content – this might warrant further investigation. The roughness length z_0 was estimated as 0.85 cm.

We started the computation with the initial conditions observed on 24 August 1953 at 12.30 a.m., and integrated for 36 hours with a time step of 10 minutes. The model has 15 unevenly spaced levels, the lowest levels being at approximately 30, 240, 640, 1230 and 2000 m.

The results are shown on Figures 2 to 7. In all the figures the observed values are connected by thin lines whereas the computed values are shown as thick curves.

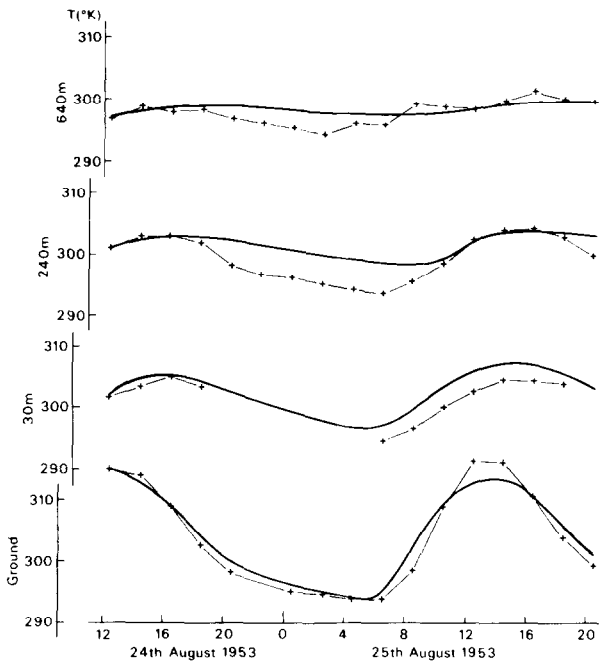

Fig. 2. Temperature at the ground and at various levels in the boundary layer, period 5 of the O'Neill experiment. Computed: —, measured: + — +.

Figure 2 shows the evolution of the temperature at the ground and at the heights corresponding to the three lowest levels of the model. The daily variation of the ground temperature is simulated quite well. At 30 m the computed temperature is a few degrees too high after 18 hours of integration. Since there are no observations at night at this level, it is not possible to tell when the computed temperature starts diverging from the observed one; however, the curves for the next two higher levels show that the difference becomes apparent early in the night. Notwithstanding the possible effect of large-scale advection, it appears that the model does not cool the atmosphere quickly enough at night. The reason might be either that the downward flux of heat in stable conditions is still too small, or that the radiative cooling is not strong enough. Nevertheless, considering the simplicity of the model and its coarse vertical resolutions, these results are encouraging.

Similarly the simulation of the relative humidity at the ground (Figure 3), and the time variation of the mixing ratio at 30 m (Figure 4) are quite satisfactory. Figure 5 shows that, even though keeping the geostrophic wind constant is an oversimplified assumption, the computed stress at the ground compares favourably with the value

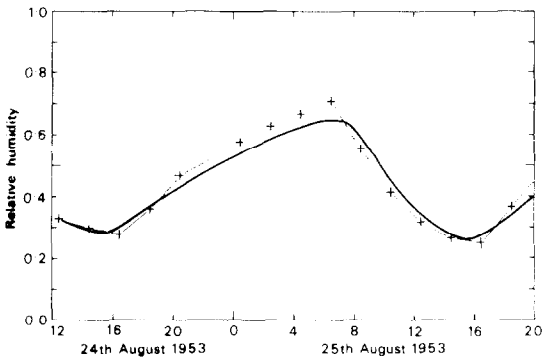

Fig. 3. Ground relative humidity, period 5 of the O'Neill experiment. Computed: ———, measured +———+.

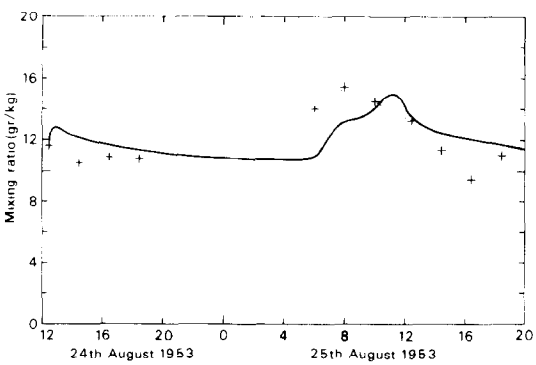

Fig. 4. Water vapour mixing ratio at 30 m, period 5 of the O'Neill experiment. Computed: ———, measured: +———+.

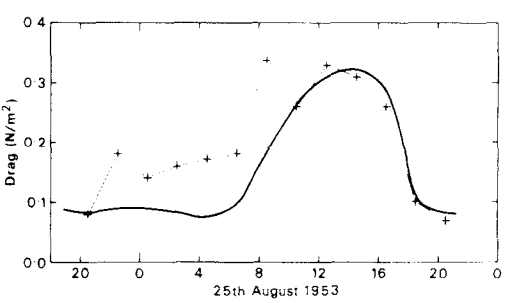

Fig. 5. Surface shear stress, period 5 of the O'Neill experiment. Computed: ———, measured: +———+.

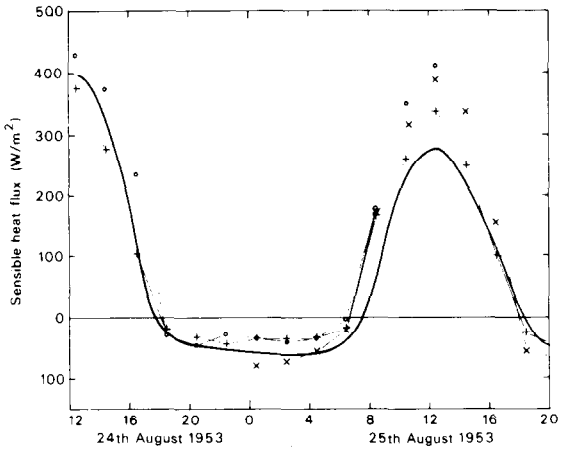

Fig. 6. Sensible heat flux at the ground, period 5 of the O'Neill experiment. Computed: ———, estimated by Lettau: +———+, Suomi: ○———○ and Halstead: ×———×.

measured with a drag plate. There are no direct measurements of the surface eddy fluxes of sensible or latent heat during the O'Neill experiment, but they were estimated by three different methods by Lettau, Suomi and Halstead (Lettau and Davidson, 1957). In Figures 6 and 7, the results of the present computation are compared with these estimates. There is good agreement between the four models for the eddy flux of sensible heat, but our estimate of the latent heat flux is considerably higher than the other three during the day. If we integrate the latent heat flux over the day, we can obtain the net amount of water added to the atmosphere. The difference between our estimate and the others is of the order of $1.5\,\mathrm{kg\,m^{-2}}$ or, assuming that this water is distributed roughly uniformly in the boundary layer, a difference of about 1 gr/kg. Unfortunately the measurements of the water vapour distribution are so noisy that it is impossible to establish such a difference from the data.

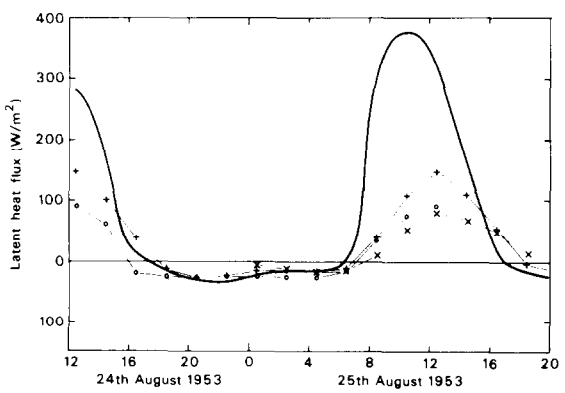

Fig. 7. Latent heat flux at the ground, period 5 of the O'Neill experiment. Computed: ———, estimated by Lettau: +———+, Suomi: ○———○ and Halstead: ×———×.

B. Strong forcing

The second experiment which we present here was designed to test the response of the model to a strong forcing. The chosen situation was first studied by Økland (1976). In this case a mass of cold arctic air moved over the Norwegian Sea and was strongly warmed and moistened as it travelled South-West. Figure 8, which is

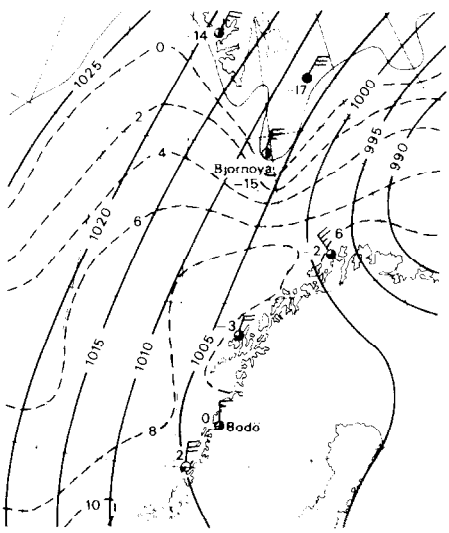

Fig. 8. Sea surface temperature and surface maps for 21 November 1975, 12 GMT. (Adapted from Økland, (1976).)

adapted from Økland's work, shows the synoptic situation at the surface and the sea surface temperature for 21 November 1975. The extent of the sea ice is shown by the hatched area. A mass of air leaving the ice at Björnöya would reach a point over the sea off Bodö about 18 hours later. Since there was very little shear or deformation in the large-scale flow, we can assume that most of the changes in the air mass were due to exchanges with the sea, vertical eddy fluxes, and the release of latent heat. This again permits us to use a one-dimensional model to simulate the evolution of the atmospheric structure. Figure 9 shows the soundings for temperature and dew point temperature at Björnöya and Bodö on 21 November 1975 at 00 and 12 GMT, respectively on a skew-T, log p diagram. These soundings are taken as representative of the air at the beginning and at the end of its trajectory.

This kind of synoptic pattern happens fairly frequently in winter, and it is an example of a situation in which the diabatic transformations can interact strongly with the large-scale flow. Økland has shown that differential heating over the sea and the continent leads to the development of a characteristic trough, frequently associated with such outbreaks of polar air. Hence it is important to be able to forecast this phenomenon accurately.

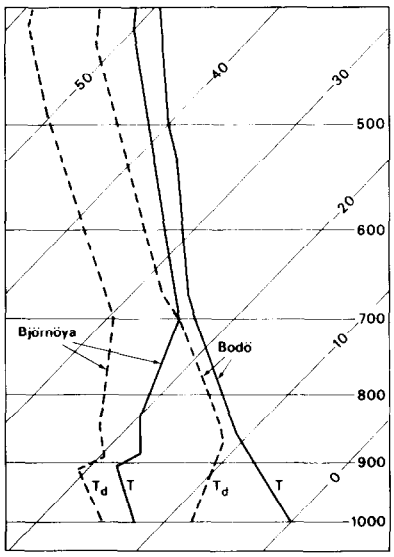

Fig. 9. Skew-T/log p diagram of temperature and dew-point temperature at Björnöya and Bodö for 21 November 1975. (From Økland (1976).)

We use Björnöya's sounding as initial conditions and, integrating the model for 18 hours, with constant geostrophic wind and imposed sea surface temperature, we compare the results with the sounding at Bodö. In this case we have to add a simulation of the moist processes to the model described above. The large-scale rain is simulated very simply by raining out any supersaturated water. For the moist convection, we use the scheme developed by Kuo (1965).

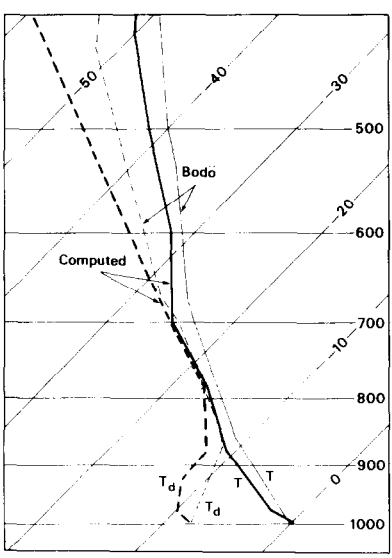

Fig. 10. Result of the computation, compared with the sounding at Bodö.

The results of the computation are shown on Figure 10 where we compare the computed temperature and dew-point temperature with the sounding at Bodö. These results are quite satisfactory: the net heating and moistening of the boundary layer is very well reproduced and the vertical structure of the temperature and humidity curves is quite similar to the one observed. It could be argued that the moisture has not been increased enough above 600 mb, but at these low temperatures, even the observed humidity is probably not very accurate.

It must be mentioned that the dependence of the diffusion coefficients on the static stability is essential to the correct simulation of this air mass transformation. For comparison, we show on Figure 11 the results of a computation using a simpler model

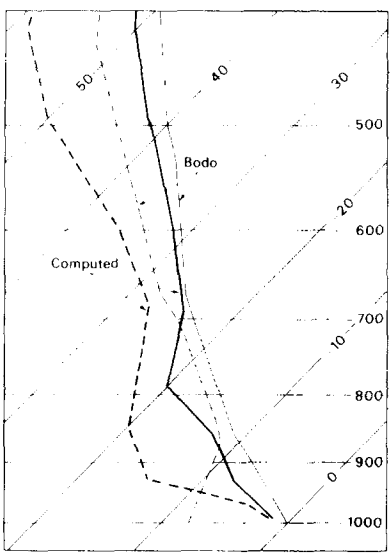

Fig. 11. Same as Figure 10, but computation done with a simpler model.

in which the diffusion coefficients are imposed as function of height only (see Smagorinsky *et al.*, 1965). It can be seen that this model is unable to transport water vapour upwards fast enough. The resulting dew-point temperature curve is quite wrong.

It should be noted also that although our model has no explicit dry adiabatic adjustment, the super-adiabatic lapse rates which are allowed to exist do not become very large, even when the surface temperature is much higher than the air temperature.

4. Conclusions

We have shown that a simple model of the planetary boundary layer, using surface fluxes and diffusion coefficients which depend on shear and stability, is able to

simulate the diurnal cycle, as well as to respond correctly to a very strong forcing from the surface. In the two tests presented here, the vertical structure and the time evolution of the temperature and humidity were well reproduced. The variations of the surface stress were also well simulated. This formulation is now being tested in a global forecast model.

Acknowledgment

The author wishes to thank especially M. Tiedtke and J. F. Geleyn for their help in developing this model.

References

Arya, S. P. S. and Sundararajan, A.: 1976, 'An Assessment of Proposed Similarity Theories for the Atmospheric Boundary Layer', *Boundary-Layer Meteorol.* **10**, 149–166.

Barker, E. H. and Baxter, T. L.: 1975, 'A Note on the Computation of Atmospheric Surface Layer Fluxes for use in Numerical Modelling', *J. Appl. Meteorol.* **14**, 620–622.

Bhumralkar, C. M.: 1975a, 'Parameterization of the Planetary Boundary Layer in Atmospheric General Circulation Models. – A review. Report R-1654-ARPA, Defense Advanced Research Projects Agency, Order No. 189-1, RAND.

Bhumralkar, C. M.: 1975b, 'Numerical Experiments on the Computation of Ground Surface Temperature in an Atmospheric General Circulation Model', *J. Appl. Meteorol.* **14**, 1246–1258.

Busch, N. E., Chang, S. W., and Anthes, R. A.: 1976, 'A Multi-Level Model of the Planetary Boundary Layer Suitable for Use in Mesoscale Dynamic Models', *J. Appl. Meteorol.* **15**, 909–919.

Businger, J. A., Wyngaard, J. C., Izumi, Y., and Bradley, E. F.: 1971, 'Flux-Profile Relationship in the Atmospheric Surface Layer', *J. Atmos. Sci.* **28**, 181–189.

Carson, D. J. and Richards, P. J. R.: 1978, 'Modelling Surface Turbulent Fluxes in Stable Conditions', *Boundary-Layer Meteorol.* **14**, 68–81.

Clarke, R. H.: 1970, 'Recommended Methods for the Treatment of the Boundary Layer in Numerical Models', *Aust. Meteorol. Mag.* **18**, 51–73.

Deardorff, J. W.: 1972, 'Parameterization of the Planetary Boundary Layer for Use in General Circulation Models', *Mon. Wea. Rev.* **100**, 93–106.

Deardorff, J. W.: 1978, 'Efficient Prediction of Ground Surface Temperature and Moisture, with Inclusions of a Layer of Vegetation', *J. Geophys. Res.* **83**, 1889–1903.

Delsol, F., Miyakoda, M., and Clarke, R. H.: 1971, 'Parameterized Processes in the Surface Boundary Layer of an Atmospheric Circulation Model', *Quart. J. Roy. Meteorol. Soc.* **97**, 181–208.

Dyer, A. J.: 1974, 'A Review of Flux-Profile Relationships', *Boundary-Layer Meteorol.* **7**, 363–372.

Geleyn, J.-F. and Hollingsworth, A.: 1979, 'An Economical Analytical Solution for the Interaction Between Scattering and Line Absorption of Radiation', To appear in *Beitr. Phys. Atmos.*

Högström, U. and Smedman-Högström, A. S.: 1974, 'Turbulence Mechanisms at an Agricultural Site', *Boundary-Layer Meteorol.* **7**, 373–389.

Kondo, J., Kanechika, O., and Yasuda, N.: 1978, 'Heat and Momentum Transfers under Strong Stability in the Atmospheric Surface Layer', *J. Atmos. Sci.* **35**, 1012–1021.

Kuo, H. L.: 1965, 'On Formation and Intensification of Tropical Cyclones Through Latent Heat Release by Cumulus Convection', *J. Atmos. Sci.* **22**, 40–63.

Lettau, H. H. and Davidson, B.: 1957, *Exploring the Atmosphere's First Mile*, Vol. 2, Pergamon Press, New York, 578 pp.

Merrill, J. T.: 1977, 'Observational and Theoretical Study of Shear Instability in the Airflow near the Ground', *J. Atmos. Sci.* **34**, 911–921.

Monin, A. S. and Obukhov, A. M.: 1954, 'Basic Regularity in Turbulent Mixing in the Surface Layer of the Asmosphere', *Akad. Nauk. S.S.S.R. Trud. Geofiz. Inst., Tr.* **24**, 163–187.

Økland, H.: 1976, 'An Example of Air-Mass Transformation in the Arctic and Connected Disturbances of the Wind Field', University of Stockholm, Dept. of Meteorology. Report No. DM-20.

Paulson, C. A.: 1970, 'The Mathematical Representation of Wind Speed and Temperature Profiles in the Unstable Atmospheric Surface Layer', *J. Appl. Meteorol*, **9**, 857–861.

Phelps, G. T. and Pond, S.: 1971, 'Spectra of the Temperature and Humidity Fluctuations and of the Fluxes of Moisture and Sensible Heat in the Marine Boundary Layer', *J. Atmos. Sci.* **28**, 918–928.

Smagorinsky, J., Manabe, S., and Holloway, J. L., Jr.: 1965, 'Numerical Results from a 9-Level General Circulation Model of the Atmosphere. *Mon. Wea. Rev.* **93**, 727–768.